

## 2D SURFACE ELEVATION MEASUREMENTS BY MEANS OF X-BAND RADAR

### AN APPLICATION OF WAMOS II AT DUCK

Katrin Hessner, Konstanze Reichert, and Jens Dannenberg  
OceanWaveS GmbH, Lueneburg, Germany  
Email: [hessner@oceanwaves.de](mailto:hessner@oceanwaves.de)

Kent Hathaway, Don Resio  
Engineering Research Development Center, US Army Corps of Engineers, USA

#### 1. INTRODUCTION

The Wave and Surface Current Monitoring System WaMoS II was developed for real time measurements of directional ocean wave spectra. The WaMoS II system uses data output from a standard marine X-Band radar generally used for navigation and ship traffic control. The WaMoS II analysis consists of two steps: in the first step WaMoS II digitises the analogue radar signals, and in the second step the digital radar signatures of the sea surface are analysed and unambiguous directional wave spectra are obtained. WaMoS II can be installed on fixed platforms as well as on board vessels. The system works in real time and has proven to be especially useful under harsh weather conditions and during night when no visual observations are possible. Various WaMoS II data comparisons with in-situ wave data exist from offshore platforms, vessels, and from coastal stations (Nieto et al., 1999, Vogelzang et al., 2001, Hessner et al., 2001). Recent studies of coastal WaMoS II installations have shown that the local environment and wind conditions may influence the determination of significant wave height ( $H_s$ ) from WaMoS II measurements (Skey et al., 2006).

In this paper the results of a temporary WaMoS II installation at the U.S. Army Corps of Engineers (USACE) Field Research Facility (FRF), in Duck, NC, USA (Lat: 36° 10' 57" N, Lon: 75° 45' 50" W) are discussed. The paper is separated into two parts. Part one deals with the WaMoS II spectral wave parameters. The WaMoS II wave measurements are compared with independent in-situ wave data. A correlation between WaMoS II  $H_s$  and wind speed and direction is found. The results of a wind correction to the values of  $H_s$  are presented.

In part two, sea surface elevation maps obtained by a new WaMoS II software tool are presented. In contrast to spectral wave measurements, sea surface elevation maps allow investigation of individual waves in time and space. Within the EU funded project *MaxWave*<sup>1</sup> several inversion algorithms for nautical and satellite radar data were developed (Nieto et al., 2004, Dankert & Rosenthal, 2004, Schulz-Stellenfleth & Lehner, 2004). Here, a brief

---

<sup>1</sup> MaxWave: Rogue waves - Forecast and impact on marine structures, EVK3-CT-2000-00026

overview of one inversion scheme for nautical radar images (Nieto et al., 2004) is presented. Further, a comparison between WaMoS II sea surface elevation maps and pressure gauge elevation data is shown.

## 2. WAMOS II INSTALLATION AT DUCK

From February to October 2005 WaMoS II was installed at Duck. WaMoS II was connected to a Furuno FR-7112 X-Band radar fitted with a 6 feet open antenna. The radar repetition rate was 2.5 s (24 rpm). The radar images covered a range from 240 m to 2160 m with a spatial resolution of about 7.5 m. WaMoS II was set-up to analyse a sequence of 64 radar images. The wave analysis was carried out for two rectangular (128 x 256 pixel) analysis areas, located about 850 m to 1810 m from the radar antenna. These locations are generally outside the surf zone, so that linear wave theory is applicable in the data processing. Furthermore, they are located outside of the area with irregular bathymetry around the pier and the near shore bar system. The wave spectra are determined separately for both analysis areas and then spectrally averaged. This is to minimize bathymetry induced in-homogeneities in the wave field and to obtain more statistical stability for the near-shore sea state. The wave parameters significant wave height, peak wave period and direction and wave length are derived from these spectra. The resulting WaMoS II wave parameters are updated every 5 minutes and represent spatial means of 3.7 km<sup>2</sup> and temporal means of 2.7 minutes. For better comparisons with in-situ wave data the WaMoS II wave data are also temporally averaged over 30 minutes.

Figure 1 shows the location of the USACE, Field Research Facility (FRF), in Duck, NC, USA. The enlarged area shows an example of a WaMoS II X-Band radar image. The colour coding of the radar image corresponds to the radar backscatter strength, where black indicates no radar return and white maximum radar return. Here, most radar signals are caused by land structures. The pier is visible as a line of enhanced radar backscatter relative to the sea surface. The white boxes indicate the size and position of the two WaMoS II wave analysis areas. The locations of the reference sensors: Anemometer (Gauge ID 3932), Waverider buoy (Gauge ID 630), and pressure gauge (Gauge ID 3111) are indicated by red dots. Note, that the coast-line at Duck is aligned about 160° (340°) relative to North.

The anemometer is located about 19 m above sea level at the end of the pier and delivers wind speed and direction. The wind data is sampled at 2 Hz. The output is 34 minute averaged vector data. The wind direction is given relative to North and indicates the direction from which the wind is blowing.

The Waverider buoy is located about 4.8 km south-east of the pier and provides significant wave height ( $H_s$ ), peak wave period ( $T_p$ ), and peak wave direction ( $\Theta_p$ ). The Waverider  $H_s$  is defined as an energy-based statistic equal to four times the standard deviation of the sea surface elevation. The data is sampled at 2 Hz over 34 minutes.

The pressure sensor is a Senso-Metric Model SP973(C) and is located approximately 0.5 m off the sea bottom in the vicinity of the 8 m isobar which is about 975 m north-east from the radar location. The data received from the pressure gage are in the form of a time series of the water depth from the pressure gage to the sea surface. The data is sampled at 2 Hz over 34 minutes.

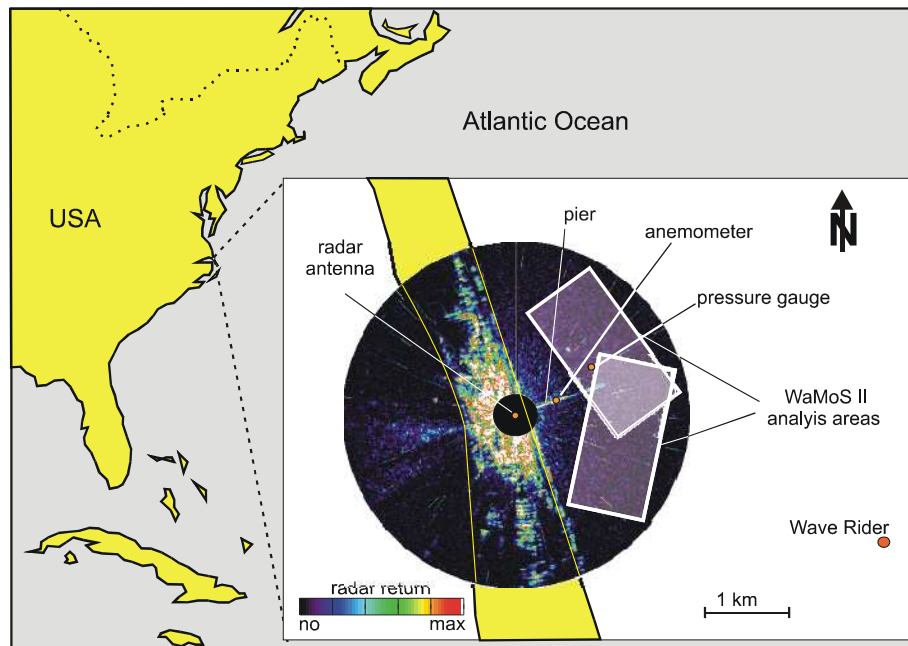


Figure 1: Location of the USACEFRF, in Duck, NC, USA: The enlarged area is an example of a WaMoS II X-Band radar image. The white boxes indicate the position of the WaMoS II wave analysis areas. Red dots mark the location of the reference sensors: anemometer, pressure gauge, and Waverider.

### 3. SPECTRAL WAVE DATA

For the comparison between WaMoS II and the Waverider, the main statistical sea state parameters of significant wave height ( $H_s$ ), peak wave period ( $T_p$ ), and peak wave direction ( $q_p$ ) are used. WaMoS II derives  $T_p$  and  $q_p$  directly from the wave spectra, while  $H_s$  is determined indirectly from the signal to noise ratio in the radar images (Nieto, 1998). In the following analyses, wave data from September 2005 is presented because during this period a variety of different sea states and wind conditions were observed.

In Figure 2 the time series of the sea state parameters  $T_p$  (upper panel) and  $q_p$  (lower panel) for Sep. 2005 are shown. The red dots refer to the WaMoS II peak wave parameters and the blue dots to the Waverider buoy measurements. 'WaMoS II data for which the radar signals were too weak for WaMoS II wave measurements are marked in grey. In addition to the peak wave parameters obtained by WaMoS II, the corresponding swell (wave periods above 10s, green) and wind sea (wave periods below 10s, purple) are shown. The grey boxes indicate periods in which WaMoS II observed bi-modal sea states with significant wind sea and swell wave systems.

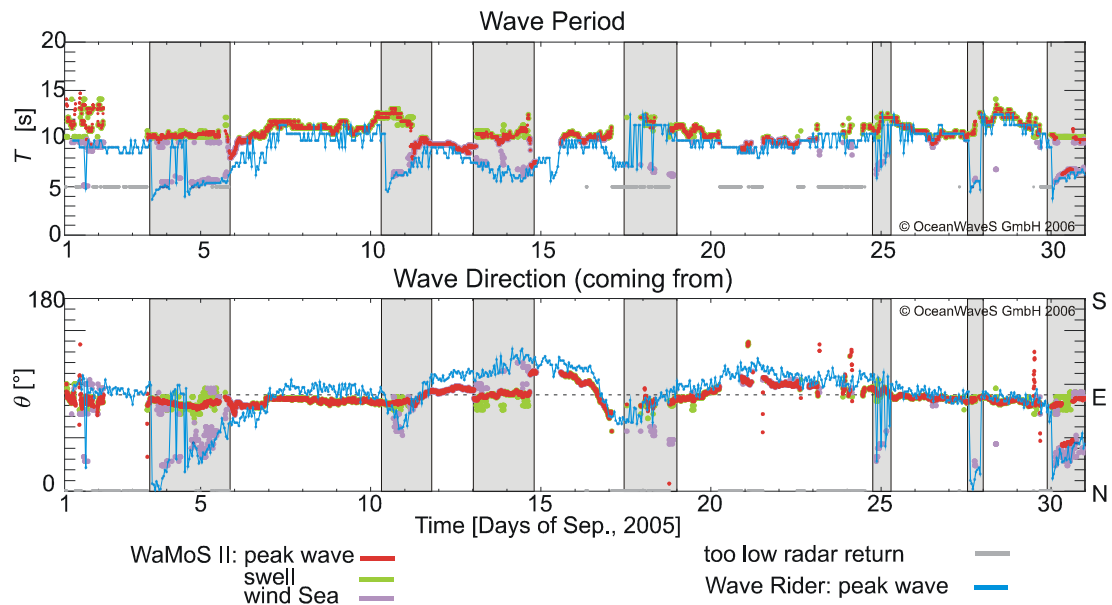


Figure 2: Time series of peak wave period ( $T_p$ ) and direction ( $q_p$ ) obtained by WaMoS II (red) and the moored buoy (blue). The periods and directions for swell and wind sea as measured by WaMoS II are given in green and purple, respectively. Radar measurements with too low radar signals for wave measurements are marked grey.

Both  $T_p$  and  $q_p$  show an excellent agreement between the measurements of the two sensors. When there is a bi-modal sea the sensors sometimes give different peak wave properties. This is well explained by the differences in the two measuring principles: the Waverider buoy delivers temporal means of a point measurement, 4.8 km off-shore in relative deep water, while WaMoS II data represents spatial and temporal means near the coast with an average water depth of 8 m. This causes systematic *natural* differences between the measurements of the two sensors. In cases of a bi-modal sea these differences are somehow amplified as the two sensors may determine different wave systems as the dominate peak wave system. Nevertheless, the time series shows that WaMoS II always detects the Waverider peak wave system. For example, in the first bi-modal period (Sep. 3-6<sup>th</sup>) WaMoS II measures two wave systems: A swell with  $T = 10\text{s}$ ,  $\vartheta \approx 80^\circ$  and a wind sea system with  $T = 4\text{-}6\text{s}$ ,  $\vartheta \approx 40^\circ$ . In this period the peak wave parameters determined by the Waverider alternate between the swell and the wind sea, while WaMoS II regards the swell as the dominant peak wave system all the time.

In Figure 3 the  $H_s$  measurements from WaMoS II and the Waverider, as well as the wind measurements from the anemometer are shown. The upper panel of Figure 3 shows the time series of  $H_s$ , where red refers to the WaMoS II measurements and blue to those from the Waverider. For the times with too low radar backscatter WaMoS II  $H_s$  is set to 0.5m and marked grey. In the two lower panels the corresponding time series of wind speed ( $W$ ) and direction ( $q_w$ ) are shown. In the upper and middle panel the grey boxes highlight the periods when the WaMoS II and Waverider measurements agree very well. In the lower panel the grey area marks the offshore wind directions ( $160^\circ < q_w < 340^\circ$ ). Here, offshore wind means wind

blowing from the shore towards the sea in contrast to onshore winds which blow from the sea towards the shore. The  $H_s$  time series in Figure 3 shows four storm events (Sep. 5<sup>th</sup> -7<sup>th</sup>, 10<sup>th</sup> -12<sup>th</sup>, 15<sup>th</sup>-17<sup>th</sup> and 25<sup>th</sup>-26<sup>th</sup>) where  $H_s$  ranges from 1 m to 3 m. In the periods of Sep. 2<sup>nd</sup>-3<sup>rd</sup> and 17<sup>th</sup>-25<sup>th</sup> the sea state was calm with  $H_s$  below 0.8 m. The wind conditions for these times can mainly be separated into two periods: Between Sep. 3<sup>rd</sup> -17<sup>th</sup> the wind was directed onshore with wind speeds up to 15m/s and for the rest of the time the wind speed was relatively low (1-6m/s) with clockwise turning wind directions.

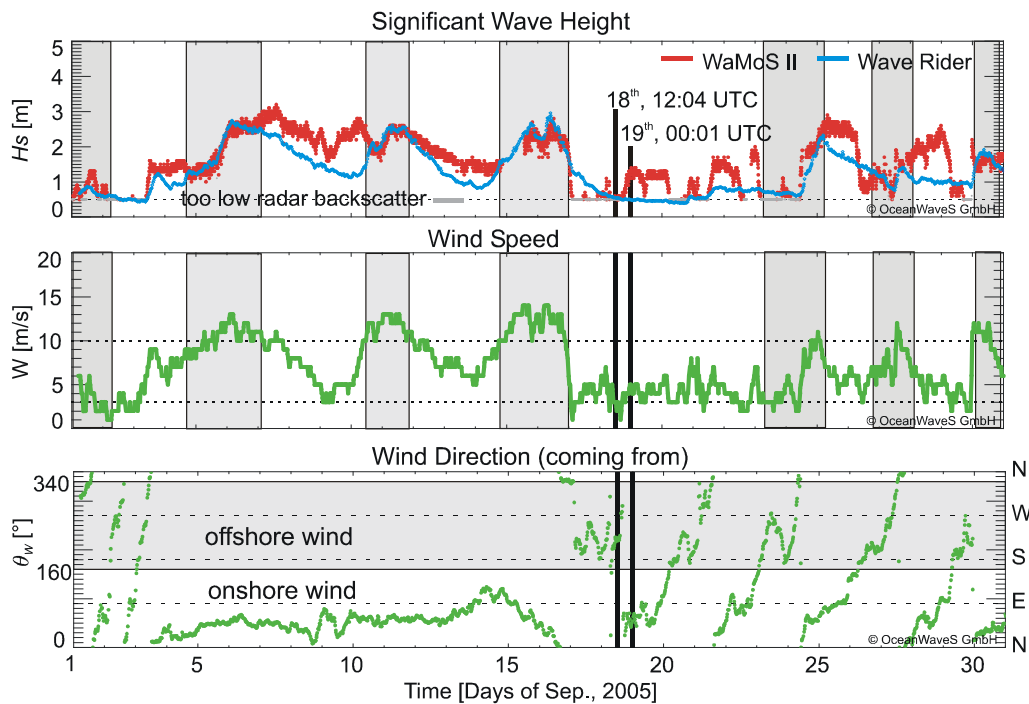


Figure 3: Time series for Sep. 2005. Top:  $H_s$  from WaMoS II (red) and Waverider buoy (blue). Wind speed ( $W$ ; middle) and direction ( $q_w$ ; bottom) from the anemometer at Duck pier.

In contrast to the previously discussed wave parameters ( $T_p$  and  $q_p$ ), both  $H_s$  time series show only episodic agreement. In general, the periods of agreement coincide with growing sea (increasing  $H_s$ ). The times when WaMoS II gives a value of  $H_s$  greater than the Waverider mainly occur when  $H_s$  is decreasing. Further, a correlation between the level of agreement and the wind is apparent.

In Figure 4 the  $H_s$  variations between WaMoS II and the Waverider buoy are shown with respect to the wind direction (Figure 4, left) and wind speed (Figure 4, right). In the wind direction plot it can be seen that the highest variations of about 0.7m are observed for low onshore wind situations, while for moderate onshore winds ( $W > 10$  m/s) and low offshore wind situations both sensors show a good agreement. In the wind speed plot the  $H_s$  variations for onshore wind situations show an almost linear dependency with the wind speed. The

highest deviations were observed at  $W = 5$  m/s. With increasing wind speed the variation decreases and for  $W > 10$  m/s both  $H_s$  measurements are in good agreement. For lower wind speeds ( $W < 5$  m) the agreement increases again with decreasing wind speed. For offshore winds the agreement is almost independent from the wind speed (note that for offshore wind situation no wind speeds higher than 10 m/s were observed).

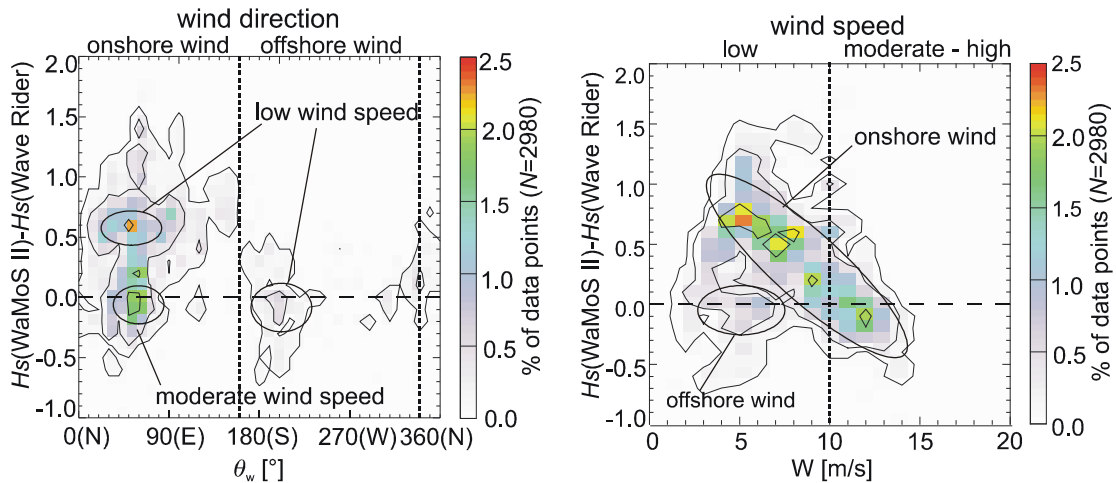


Figure 4:  $H_s$  variations between WaMoS II and Waverider with respect to wind direction (left) and wind speed (right) for Sep. 2005.

To better understand the wind dependency of the variation of  $H_s$  between WaMoS II and Waverider the imaging mechanism of surface waves in radar images must be considered.

#### 4. RADAR WAVE IMAGING MECHANISM

The wave patterns in nautical radar images are radar echoes (sea clutter) from the rough sea surface (Bragg scattering; Lee et al., 1995). For nautical X-Band radars this sea surface roughness corresponds to ripple (Bragg) waves with a wave length in the range of 2-5 cm. The generation and presence of these ripples is directly correlated with the wind speed. The longer sea surface waves like wind sea (5-10 s) and swell ( $>10$  s) become visible in the radar images by the modulation of the sea clutter due to shadowing, hydro-dynamic, and tilt modulation (Alpers et al., 1981). In contrast to *in-situ* wave sensors, WaMoS II determines the significant wave height ( $H_s$ ) indirectly from the signal to noise ratio (Nieto, 1998), where the signal corresponds to the wave energy of the long sea surface waves (wind sea and swell) and the noise corresponds to residual energy, which is mainly related to the general strength of the sea clutter.

The dependency of the radar backscatter on wind speed and wind direction relative to the radar look direction has been investigated theoretically and empirically in several studies (e.g.

Schroeder et al., 1982, Romeiser et al., 1997, Plant et al., 1999). They found that in up-wind cases the radar signatures of long surface waves (wind sea and swell) are stronger than for down-wind situations. This difference can also be seen in the following two nautical radar images obtained by WaMoS II at Duck (see Figure 5).

Both radar images were acquired when the buoy and the WaMoS II measured an  $H_s$  of about 0.5 m and the wind speed was 3 m/s and 4 m/s, respectively. The left panel of Figure 5 shows an offshore wind situation with almost no radar signatures of the sea surface. At this time the  $H_s$  measurements of WaMoS II and Wave Rider agree very well.

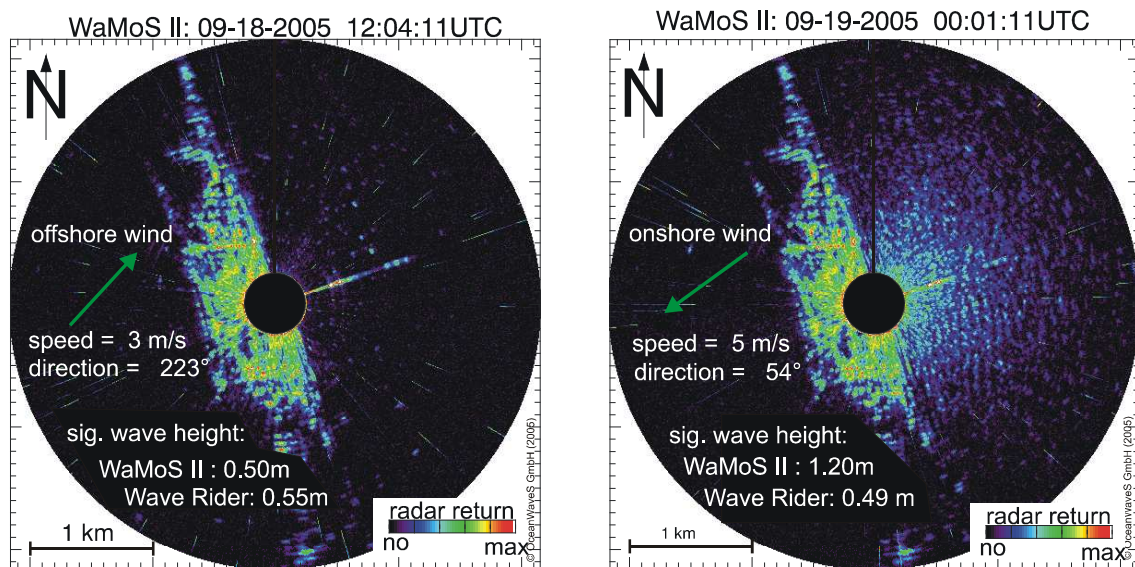


Figure 5: X-Band radar image as captured by WaMoS II on Sep. 18, 2005, 12:04 UTC during offshore wind condition (left) and on Sep. 18, 2005, 00:01 UTC during onshore wind condition (right). The green arrow indicates the wind direction.

The right panel of Figure 5 shows an onshore wind situation. The radar image exhibits clear radar signatures of westward propagating sea surface waves. Since the calculated  $H_s$  depends directly on the intensity of the wave signatures this effect leads to increased  $H_s$  values during onshore wind situations. For this example WaMoS II yields an  $H_s$  of about 0.7 m higher than the Waverider. For moderate wind speeds ( $W \approx 5$  m/s) this effect is enhanced. For growing wind speeds this effect reaches saturation and only a dependence of the wind direction can be observed.

#### 4.1 Wind correction

For WaMoS II off-shore and ship installations this wind effect has not been observed as several analysis windows can be selected covering the full 360° radar view. By averaging the

results of the different windows the wind direction dependency is suppressed. This has been shown by many previous data comparisons between WaMoS II and buoy measurements. At a coastal installation, like Duck this directional averaging over the full  $360^\circ$  is not possible.

To obtain wind independent  $H_s$  measurements for coastal applications an internal correction was developed. For this correction simultaneous wind measurements are used to account for wind direction and wind speed. Figure 6 shows the times series of  $H_s$  from the WaMoS II (red), the Waverider (blue) and the wind corrected  $H_s^*$  values from the WaMoS II data (green).

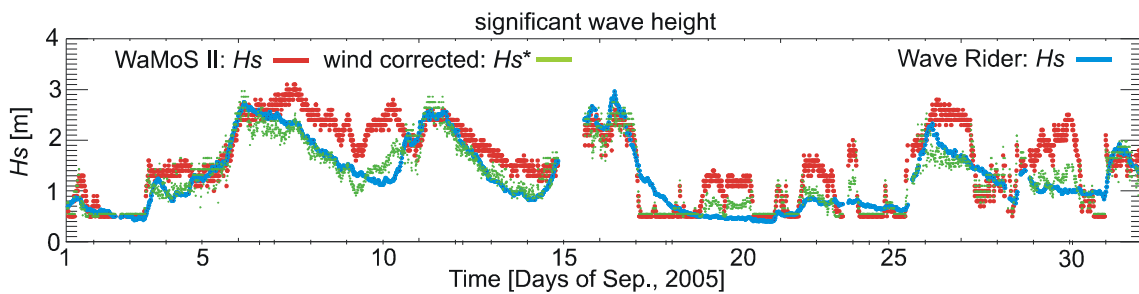


Figure 6: Time series of  $H_s$  as originally obtained by WaMoS II (red) and Wave Rider buoy (blue) and wind corrected  $H_s^*$  WaMoS II for Sep. 2005.

The wind corrected  $H_s^*$  time series shows a good agreement with the Waverider  $H_s$  measurements for the entire time series regardless of the prevailing wind situation.

The correlation between WaMoS II and Waverider measurements is improved considerably by this wind correction. This is demonstrated by the scatter plots shown in Figure 7 which give the linear correlation, root mean square error, and bias between WaMoS II and Waverider measurement for the uncorrected WaMoS II data set (left panel) and wind corrected data set (right panel).

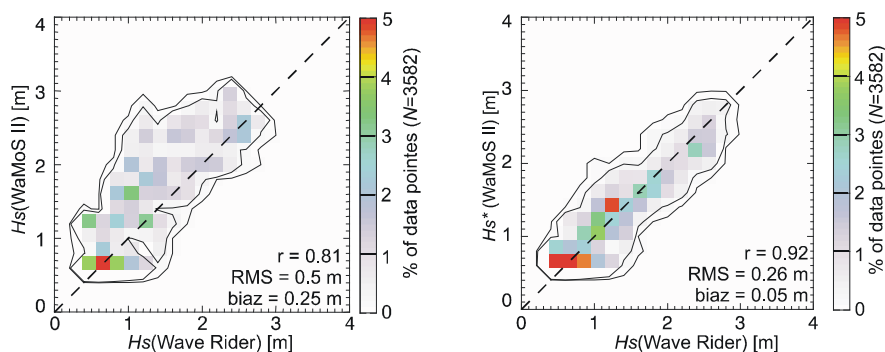


Figure 7: Uncorrected WaMoS II  $H_s$  against Waverider  $H_s$  (left) and wind corrected  $H_s^*$  WaMoS II against Waverider  $H_s$  (right) for Sep. 2005.

## 5. SEA SURFACE ELEVATION MAPS

### 5.1 Inversion scheme

To retrieve sea surface elevation maps, sequences of nautical radar images are inverted applying the method proposed by Nieto et al. (2004). This approach considers shadowing to be the main imaging mechanism of ocean gravity waves (wind sea and swell) in nautical radar images and is based on linear wave theory. It is assumed that the sea surface elevation consists of a linear superposition of several individual sinusoidal waves. By means of a FFT, a band pass filter based on the gravity wave dispersion relation, and the application of a transfer function, amplitude ( $A_i$ ) and phase ( $\phi_i$ ) of a number ( $N$ ) of individual sinusoidal waves are determined. The surface elevation ( $\eta$ ) is then given by

$$\eta(\mathbf{x}, t) = \sum_{i=1}^N A_i \cos(\mathbf{k}_i \mathbf{x} - \omega_i t + \phi_i), \quad (1)$$

where  $\mathbf{x}$  is the position vector,  $t$  the time,  $\mathbf{k}$  the wave vector,  $\omega$  the angular wave frequency.

### 5.2 Data comparison

For the comparison a time was chosen when Waverider, pressure gauge and WaMoS II measured about the same  $H_s$ .

The left panel of Figure 8 shows the radar image obtained by WaMoS II at Duck on Sep. 6, 2006, 6:03 UTC. The color coding of the radar image is related to the radar backscatter strength, where black indicates no radar return, and white refers to maximum radar return. Note, that the land area is highlighted. In the image signatures of the waves are clearly visible as stripe-like patterns. At that time the wind was blowing at 12m/s from the NE. WaMoS II measured a sea state of  $H_s = 2.5\text{m}$ ,  $T_p = 9.9\text{ s}$  and  $\Theta_p = 80^\circ$  (Waverider:  $H_s = 2.7\text{m}$ ,  $T_p = 8.5\text{s}$  and  $\Theta_p = 73^\circ$ ).

The right panel of Figure 8 shows the corresponding sea surface elevation map as obtained by WaMoS II for Sep. 6, 2006, 6:03 UTC. The colour coding is related to the surface elevation, where blue indicates wave troughs and yellow/red wave crests. The location of the pressure gauge is marked with a red dot. For the reconstruction of the sea surface elevation map, the amplitudes and phases of  $N = 3960$  sinusoidal waves were determined. In the sea surface map the striped pattern of westward travelling waves are visible. Further, clusters with enhanced surface elevation representing wave groups are visible.

To compare the WaMoS II sea surface elevation at the location of the pressure gauge (Lat:  $36^\circ 11' 14.06''$  N, Lon:  $75^\circ 44' 34.39''$  W) with the data of the pressure gauge, its distance with respect to the radar antenna (Lat:  $36^\circ 10' 57''$  N, Lon:  $75^\circ 45' 50''$  W) was estimated to be 975.5 m from the antenna at an angle of  $53^\circ$  with respect to North.

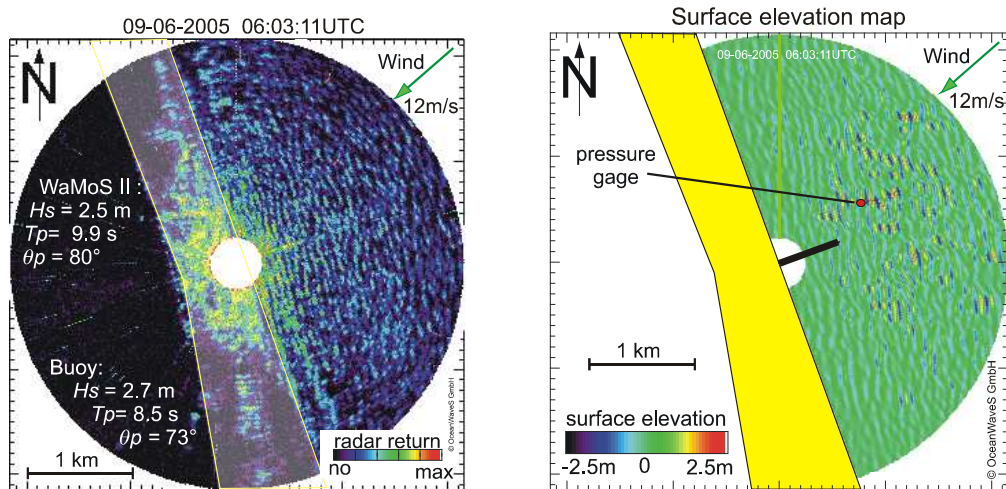


Figure 8: Left: Nautical radar image as obtained by WaMoS II on Sep. 6, 06:03 UTC. The color coding indicates the radar backscatter strength. Note, that the land area is highlighted. Right: Sea surface elevation map as obtained by WaMoS II for Sep. 6, 06:03 UTC. The color coding indicates surface elevation with blue being wave troughs and yellow/red wave crests. The land is marked yellow and the pier is a black line.

To relate the spatial and temporal evolution of the waves, temporal and spatial transects for the WaMoS II sea surface elevation are shown in Figure 9. The upper panel shows the temporal evolution of the WaMoS II sea surface for Sep. 6, 06:03 UTC over the period of 32 antenna revolutions ( $T = 32 \text{ RPT} = 84.8\text{s}$ ) at the location of the pressure gauge. The red time series has the same temporal resolution as the pressure gauge data (0.5s), while the dotted black line indicates the time series determined with the resolution given by the radar repetition time ( $\text{RPT} = 2.65\text{s}$ ). The lower panel shows the spatial transect along the wave propagation line at the time when the central wave occurred ( $T = 42.4\text{s}$ ).

Both series show a good self-consistency with respect to form and height of the individual waves. With increasing time and space from the *central* wave ( $T = 42.4\text{s}$ ,  $s = 382.5\text{m}$ ) at the pressure gauge, deviations between the temporal and spatial form of the wave can be recognized. This is caused by the different evolution of individual waves in time and space.

The pressure gauge delivers time series of the water depth from the gauge to the sea surface. To get comparable surface elevation information the mean water depth over the 34.6 minutes is determined and subtracted from the single depth measurements.

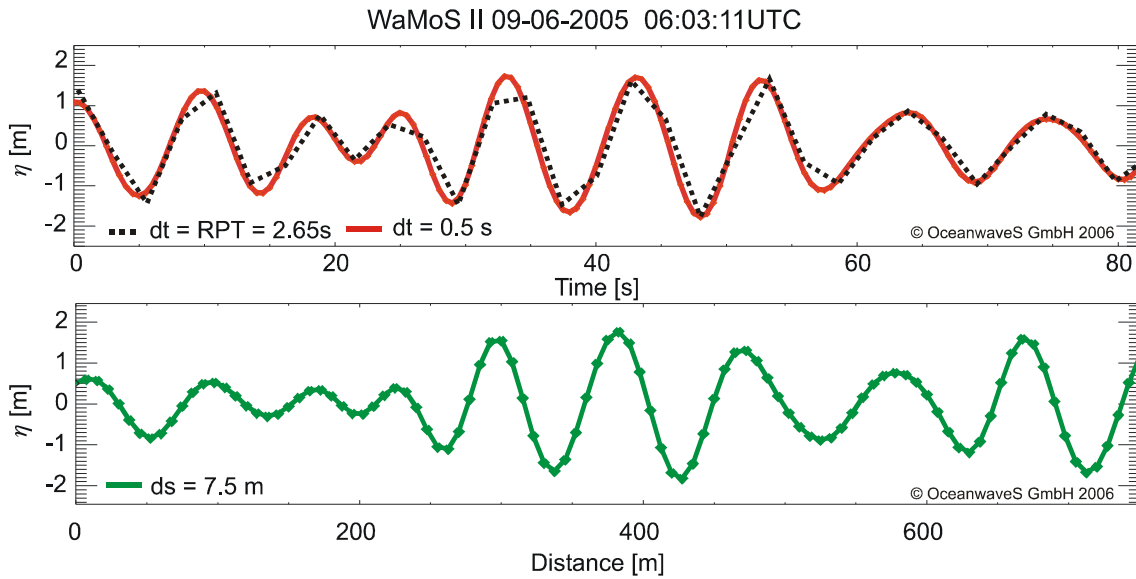


Figure 9: Temporal (upper panel) and spatial (lower panel) transects of the surface elevation as obtained by WaMoS II inversion scheme at the location at the pressure gauge.

Figure 10 shows the time series of the surface elevation obtained from the pressure gauge (blue) and by the WaMoS II inversion (red). Since the clocks of the two systems were not synchronized the time series are shifted by about 2 minutes and 39 seconds, so that the observed waves are in phase

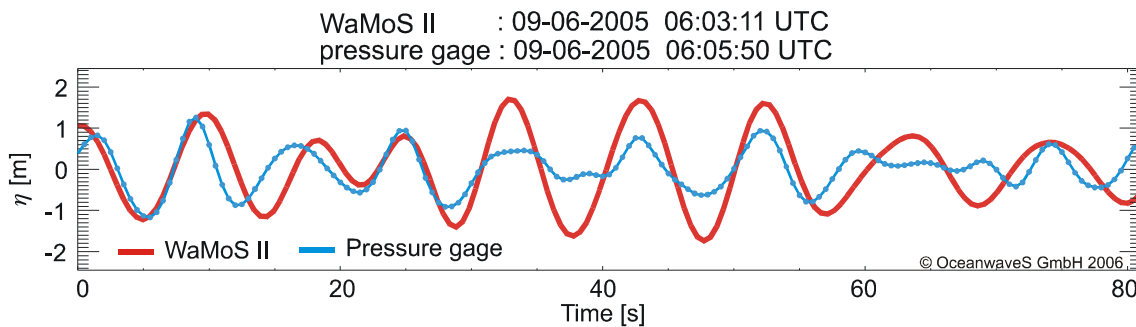


Figure 10: Time series of the sea surface elevation ( $\eta$ ) from the WaMoS II (red) and the pressure gauge (blue). Both time series are sampled at 0.5 Hz.

The periods of the waves are in good agreement while the form and height of the waves differ. These differences can be related to several factors. Two systematic errors exist because the precise location of the pressure gauge relative to the radar antenna and time lag between the WaMoS II and the pressure gauge time series are unknown. Furthermore, both sensors are based on different measuring principles. The pressure gauge data represent point measurements while the radar based sea surface maps give point information over  $7.5 \times 7.2 \text{ m}^2$ .

To validate the WaMoS II sea surface elevation data with the pressure gauge data more data sets need to be analysed and the exact temporal and spatial shift between WaMoS II and pressure gauge needs to be determined.

## 6. SUMMARY AND CONCLUSION

A comparison of spectral sea state parameters from a WaMoS II wave radar and a Waverider buoy at Duck for Sep 2005 is presented. It shows that for peak wave period and peak wave direction both sensors are in good agreement. For the significant wave height the WaMoS II measurements do not show such a good agreement but are closely correlated to the local wind speed and direction. This dependency is caused by the specific coastal set-up at Duck which results in on-shore long crested waves in conditions of both onshore and offshore winds. Using corrections for the local wind, the WaMoS Hs values can be corrected. Once corrected, the Hs values of the WaMoS Hs compare well with those of the buoy (RMS = 0.26m, Bias = 0.05m and R = 0.92).

In the paper a brief overview of a WaMoS II inversion algorithm is given. As an example a radar image and the corresponding sea surface elevation map is presented. The comparison between temporal and spatial sea surface elevation transects are self-consistent and show a reliable wave evolution. A comparison with pressure gauge sea surface data shows a phase agreement but differences in the magnitude. This comparison, though interesting, is of limited value because of the uncertainty of the precise location of the pressure gauge relative to the position of the radar antenna and the fact that neither system is synchronised.

## 7. REFERENCES

- Alpers, W., D.B. Ross, and C.L. Rufenach, 1981: On the Detectability of Ocean Surface Waves by Real and Synthetic Aperture Radar. *Journal of Geophysical Research*, 86, C7, pp. 6481-6498.
- Dankert, H. and W. Rosenthal, 2004: Ocean Surface Determination from X-band Radar-Images Sequences. *Journal of Geophysical Research - Oceans*, **109** C04016, doi:10.1029/2003JC002130.
- Hessner K., K. Reichert, J. Dittmer, J.C. Nieto Borge, and H. Günther, 2001: Evaluation of WaMoS II Wave data, *Proceedings of the Waves 2001 Conference*, Sep. 1-6, San Francisco.
- Lee, P.H.Y., J.D. Barter, K.L. Beach, C.L. Hindman, B.M. Lade, H. Rungaldier, J.C. Shelton, A.B. Williams, R. Yee, and H.C. Yuen, 1995: X-Band Microwave Backscattering from Ocean Waves. *Journal of Geophysical Research*, **100**, C2, pp. 2591-2611.
- Lehner, S., J. Schulz-Stellenfleth, A. Niedermeier, 2002: Detection of extreme waves using synthetic aperture radar images. *Geoscience and Remote Sensing Symposium, 2002. IGARSS '02. 2002 IEEE International, 24-28 June 2002*, Vol: 3, pp 1893 - 1895.
- Nieto, J. C., 1998: Significant Wave Height Estimation from Nautical Radar Data Sets, *GKSS*

- Nieto Borge, J.C., K. Hessner, and K. Reichert, 1999: Estimation of the Significant Wave Height with X-Band Nautical Radars. *Proc. OMAE Conference*.
- Nieto, J.C. G.R. Rodríguez, K.Hessner, P. I. González, 2004: Inversion of Marine Radar Images for Surface Wave Analysis. *Journal of Atmospheric and Oceanic Technology*., **21**, 1291-1300.
- Plant, W.J., P.H. Dahl, and W.C. Keller, 1999: Microwave and acoustic scattering from parasitic capillary waves. *J. Geophys. Res.*, **104**, 25853-25866.
- Reichert K., K. Hessner, J. Dannenberg, I. Traenkman, 2006: X-Band Radar as a Tool to Determine Spectral And Single Wave Properties: *Proceedings of OMAE2006 25th International Conference on Offshore Mechanics and Arctic Engineering June 4-9, 2006, Hamburg, Germany*
- Romeiser, R., W. Alpers, and V. Wisman, 1997: An improved composite surface model for the radar backscattering cross section of the ocean surface, 1. Theory of the model and optimization / validation by scatterometer data, *J. Geophys. Res.*, **102**, 25,237-25,250.
- Schroeder, L.C., D.H. Boggs, G. Dome, I.M. Halberstam, W.L. Jones, W.J. Pierson, and F.J. Wentz, 1982: The relationship between wind vector and normalized radar cross section used to derive Seasat-A satellite scatterometer winds. *J. Geophys. Res.*, **87**, 3318-3336.
- Schulz-Stellenfleth J. and S. Lehner, 2004: Measurement of 2-D Sea Surface Elevation Fields Using Complex Synthetic Aperture Radar Data . *IEEE Transactions on Geoscience and Remote Sensing*, **42**, No 6, pp 1149-1160
- Skey, S., K. Hessner, K. Reichert, J. Dittmer, I. Tränkman, D. Resio, 2006: Spectral and Individual Wave Measurements by WaMoS II at Duck, *13 th Ocean Sciences Meeting, Honolulu, Hawaii, 20-24 Feb. 2006* poster presentation OS46H-10.
- Vogelzang, J., K. Boogaard, and K. Hessner, 2001: Radar Wave Height Measurements, The use of Navigation radar for wave monitoring. Hydro International, Vol 5, No 6, 53-55.
- WMO, 1998: Guide to wave analysis and Forecasting. *WMO – No 702*.